Astron. Astrophys. 347, 194–202 (1999)

ASTRONOMY AND ASTROPHYSICS

The circumstellar molecular envelope of HD 101584

H. Olofsson[1] **and L.-Å. Nyman**[2,3]

[1] Stockholm Observatory, S-133 36 Saltsjöbaden, Sweden
[2] ESO/La Silla, Casilla 19001, Santiago 19, Chile
[3] Onsala Space Observatory, S-439 92 Onsala, Sweden

Received 18 January 1999 / Accepted 16 April 1999

Abstract. CO radio line observations reveal a molecular gas envelope around the peculiar star HD101584 with characteristics very similar to those of wellknown young post-AGB objects. We estimate that there is at least $0.1\,\mathrm{M}_\odot$ of molecular gas, very likely remnant gas from a former AGB-envelope. This gas has been efficiently accelerated to very high velocities ($>50\,\mathrm{km\,s^{-1}}$, and a significant fraction to $>100\,\mathrm{km\,s^{-1}}$). There is evidence for an expanding disk-like structure seen close to edge-on, and a high-velocity bipolar outflow. In the latter the expansion velocity increases linearly with distance from the star, suggesting either a brief period of ejection or a fast wind interacting with a slower wind. A significant fraction of the high-velocity gas has reached a welldefined terminal velocity. Momentum well above the available radiation momentum has been transferred to the gas. There are also indications of high-density, low-velocity molecular gas, possibly in a disk close to the star. The ^{12}CO/^{13}CO-ratio in the envelope is uncertain, but probably quite low ($\sim$10). The systemic heliocentric velocity is $50\pm2\,\mathrm{km\,s^{-1}}$.

Key words: stars: circumstellar matter – stars: individual: HD 101584 – stars: mass-loss – stars: AGB and post-AGB – radio lines: stars

1. Introduction

HD101584 belongs to a class of peculiar stars at moderate to high galactic latitudes with supergiant-like spectra (Waters et al. 1993). They have been intensively studied during the last decade, and there is a growing belief that most of them are low-mass post-AGB objects (Parthasarathy & Pottasch 1986; Trams et al. 1990; van der Veen et al. 1993; Bakker et al. 1996b). HD101584, was originally classified as an F-type supergiant (Humphreys 1976), but more detailed observations, of high-excitation absorption lines in the red part of the spectrum and photometry, revealed a late B-type star of higher surface gravity (Bakker et al. 1996b). The F-type spectrum probably originates in a dense stellar wind of low ionization degree. Bakker et al. (1996a) infer a 218^{d} period from photometry data, and possibly also from Doppler velocities of high-exitation absorption lines. According to the authors, the most likely explanation is the presence of a low-mass companion in a close, eccentric orbit (separation$\sim$10 R_*), but this must be regarded as only tentative. Optical emission and low-excitation absorption lines suggest the presence of a circumsystem disk (size$\sim$100 R_*) that is seen nearly edge-on (Bakker et al. 1996b). The CO first vibrational overtone bands that are seen in emission may also originate in such a disk if it is dense enough (Oudmaijer et al. 1995).

The P Cygni-profile components of the Balmer lines show that the primary star is still losing mass at a significant rate, but the estimate is uncertain, $10^{-8}-10^{-6}\,\mathrm{M}_\odot\,\mathrm{yr}^{-1}$ (Trams et al. 1990; Bakker et al. 1996b). The mass loss occurs in the form of a wind with a maximum outflow velocity of $\sim100\,\mathrm{km\,s^{-1}}$. The presence of additional absorption dips may indicate a variable mass loss. The huge far-infrared excess emission may be dominated by dust emission from an escaping circumstellar AGB-envelope. Assuming this Bakker et al. (1996b) estimate a total dust mass of $0.02\,\mathrm{M}_\odot$, and hence a total circumstellar mass probably in excess of $2\,\mathrm{M}_\odot$.

Loup et al. (1990) and Trams et al. (1990) detected a remarkable CO(J=1$\rightarrow$0) line profile from HD101584, and van der Veen et al. (1993) detected the CO(J=2$\rightarrow$1) line. The CO emission probably comes from a number of separate regions, and part of the molecular material have expansion velocities at least as high as $130\,\mathrm{km\,s^{-1}}$, i.e., considerably higher than in normal AGB-winds. A much narrower, double-peaked OH 1667 MHz maser line (maximum expansion velocity of $\sim40\,\mathrm{km\,s^{-1}}$) was detected by te Lintel Hekkert et al. (1992). The integrated OH emission is centered on the star (to within $0\farcs3$), but the data show that the gas velocity increases systematically along PA$\sim$–60° with the most blueshifted emission $\sim2''$ to the SE and the most redshifted emission at $\sim2''$ to the NW. There is no OH emission within $\sim1''$ from the star. The presence of OH emission and a 10 μm feature (Bakker et al. 1996b) suggest that the circumstellar material is O-rich (i.e., C/O$<$1).

2. Observations

We observed the ^{12}CO(J=1$\rightarrow$0 and 2$\rightarrow$1), ^{13}CO(J=1$\rightarrow$0 and 2$\rightarrow$1), SiO(v=0, J=3$\rightarrow$2), and HCN(J=1$\rightarrow$0) lines towards HD101587 in August 1997 with the Swedish-ESO Submil-

Send offprint requests to: H. Olofsson (hans@astro.su.se)

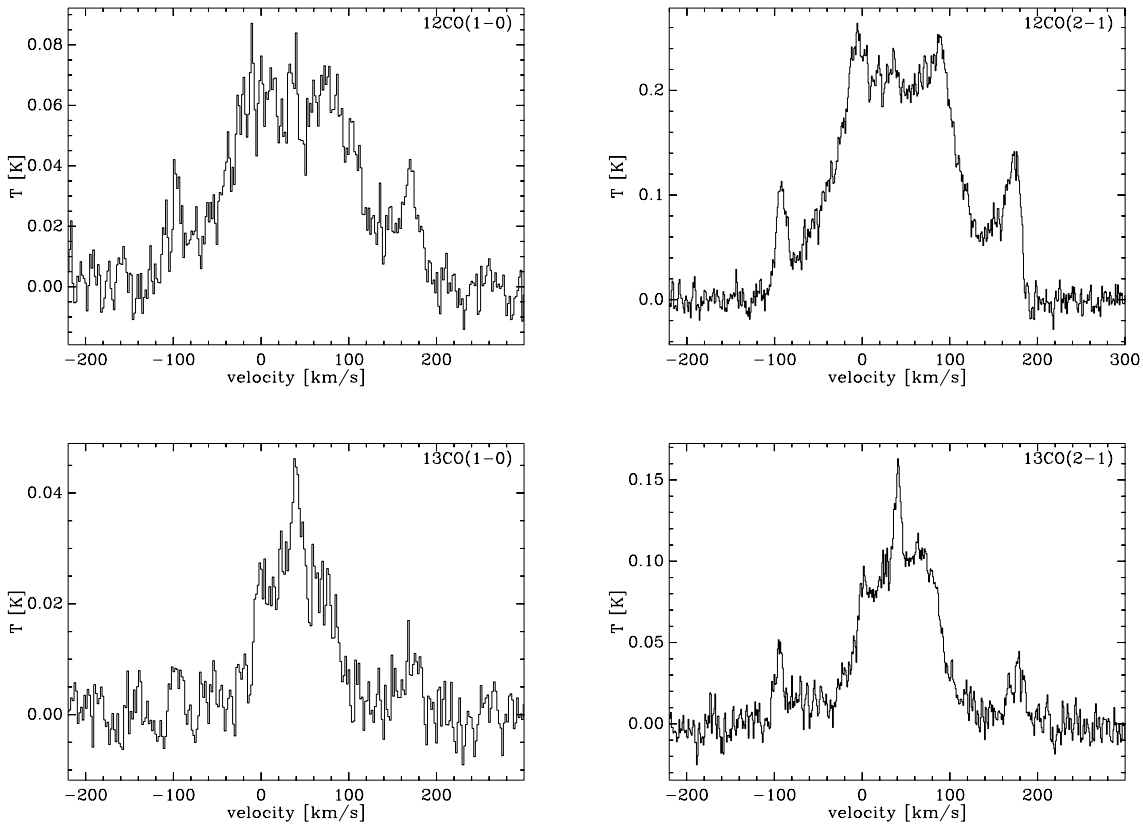

Fig. 1. ^{12}CO(J=1$\rightarrow$0 and 2$\rightarrow$1) and ^{13}CO(J=1$\rightarrow$0 and 2$\rightarrow$1) spectra obtained towards HD101584 (the map centre position spectra are shown). The intensity and velocity scales are given in main beam brightness temperature and with respect to the local standard of rest, respectively

Table 1. Telescope and receiver data

Line	Frequency [GHz]	$T_{\rm rec}^{\rm a}$ [K]	HPBW$^{\rm b}$ [″]	$\eta_{\rm mb}^{\rm c}$
HCN(J=1$\rightarrow$0)	88.6	100	57″	0.75
^{13}CO(J=1$\rightarrow$0)	110.2	130	45″	0.72
^{12}CO(J=1$\rightarrow$0)	115.3	120	44″	0.70
SiO(v=0, J=3$\rightarrow$2)	130.3	100	39″	0.67
^{13}CO(J=2$\rightarrow$1)	220.4	140	23″	0.55
^{12}CO(J=2$\rightarrow$1)	230.5	130	23″	0.50

[a] The receiver noise temperature
[b] The telescope beam full width at half power
[c] The main beam efficiency

limetre Telescope (SEST)[1], La Silla, Chile. The telescope was equipped with SIS-receivers operating in SSB-mode, and broad-band acusto-optical spectrometers with a channel separation of 0.7 MHz. The data are calibrated using the standard chopper-wheel method, and the intensity scale is given in main beam brightness temperature. The velocity scale is given with respect to the Local Standard of Rest (LSR). For HD101584 the difference between heliocentric and LSR velocity is 9.3 $\rm km\,s^{-1}$. Relevant telescope and receiver data are given in Table 1. We used the coordinates α(1950) = $11^h38^m33\overset{\rm s}{.}0$, δ(1950) = -55°17′45″ for HD101584.

The ^{12}CO(J=1$\rightarrow$0 and 2$\rightarrow$1) emissions were mapped simultaneously over an area of about 45″×40″ with a spacing of 7.″5, i.e., about 1/3 of the CO(2$\rightarrow$1) full half-power beam width (HPBW). The pointing was regularly checked on the SiO(v=1, J=2$\rightarrow$1) masers of R Car and IRSV1540, but despite this it turned out to be quite variable in the direction of HD101584. We therefore divided the data into 18 subsets (covering different parts of the map, but always including the central area), in which all data were obtained within about a 2-hour interval. For each subset we determined the position of maximum intensity (integrated over the velocity range -20 to 100 $\rm km\,s^{-1}$). Finally, all subsets were shifted [a maximum shift of 8″ was used, the average shift is 6″ and the average maximum intensity position is (-1.″5,-2.″5)], and a regridded map for each line was produced. We estimate that the centra of our final maps coincide with the position of the star to within 5″. The CO emission is essentially unresolved even at ∼20″ resolution, but we will show below that it is possible to determine relative differences in the spatial location of emission at different velocities on a scale much smaller than this.

The results obtained towards the map centre position are given in Table 2, where I=$\int T_{\rm mb} dv$, and the spectra are presented in Fig. 1. The upper limits to the HCN and SiO integrated

[1] The Swedish–ESO Submillimetre Telescope is operated jointly by ESO and the Swedish National Facility for Radio Astronomy, Onsala Space Observatory, at Chalmers University of Technology.

Table 2. Observational results towards HD101584

Line	$T_{\rm mb}$ [K]	I [K km s^{-1}]	$v_{\rm c}$ [a] [km s^{-1}]
HCN(J=1→0)		< 0.7	
^{13}CO(J=1→0)	0.04	3.3	45
^{12}CO(J=1→0)	0.07	12.3	39
SiO(J=3→2)		< 0.8	
^{13}CO(J=2→1)	0.16	13.2	41
^{12}CO(J=2→1)	0.30	41.3	44

[a] The intensity-weighted centre velocity

intensities are obtained as the peak-to-peak noise temperature, in spectra reduced to a resolution of 100 km s^{-1}, multiplied with 100 (i.e., we expect any possible HCN and SiO emission to come from the velocity range that dominates the CO emission).

3. Results

3.1. Line shapes

The discussion in this section, except in Sect. 3.5, is based on the spectra obtained towards the map centre position. The ^{12}CO(2→1) line profile has the highest S/N-ratio in our data (see Fig. 1), and a significantly higher S/N-ratio than the line profiles presented by Loup et al. (1990), Trams et al. (1990), and van der Veen et al. (1993). The line profile is well described by a weakly double-peaked central part (the Intermediate Velocity Feature, IVF, covering the central ∼100 km s^{-1}) with extended line wings (the High Velocity Wings, HVWs), and two narrow (in a relative sense) features at the extremes of the line wings (the High Velocity Features, HVFs, occasionally referred to as bHVF and rHVF, where b and r indicate blue- and redshifted emission with respect to the systemic velocity, respectively). The line profile is close to symmetric around its centre, but the line wings become somewhat asymmetric at velocities beyond ±80 km s^{-1} of the centre velocity. The bHVF is also narrower (FWHM∼15 km s^{-1}) than the rHVF (FWHM∼20 km s^{-1}). The ^{12}CO(1→0) line profile is very similar to the ^{12}CO(2→1) line profile except that the central part may be more flat-topped. The S/N-ratio of our ^{12}CO(1→0) spectrum is comparable to that obtained by van der Veen et al. (1993). The ^{13}CO line profiles, in particular the high S/N-ratio ^{13}CO(2→1) spectrum, clearly reveal an additional feature; a narrow component at the centre of the line profile (the Low Velocity Feature, LVF). Furthermore, the ^{13}CO spectra have, in a relative sense, weaker extended line wings than the ^{12}CO spectra, and the two horns seen in the central part of the ^{12}CO(2→1) spectrum are not seen in the ^{13}CO(2→1) line. When comparing with the spectra of van der Veen et al. (1993) we confirm the existence of their extreme blue- and redshifted features (features *d* and *e* in their nomenclature) and the inner peaks (features *b* and *c*), but not the intermediate high-velocity features *f* and *g*, which we believe can be attributed to the limited S/N-ratio in their spectra. The central feature *a* is not prominent enough to be safely identified in our ^{12}CO spectra, but it has the same characteristics as the LVF, which is clearly seen in the ^{13}CO spectra.

3.2. Centre velocities

The horns of the IVF part of the ^{12}CO(2→1) line profile appear at –4±2 and 88±2 km s^{-1}, i.e., they are symmetrically placed around a velocity of 42±3 km s^{-1}. The bHVF and rHVF have centre velocities of –92±1 and 173±1 km s^{-1}, respectively, as determined by fits of Gaussians profiles, i.e., they are symmetrically placed around a velocity of 41±2 km s^{-1}. The LVF of the ^{13}CO(2→1) line lies at 41±1 km s^{-1} (as estimated by a fit of a Gaussian). Thus, we estimate a systemic velocity of 41±2 km s^{-1} from the CO data (corresponding to a heliocentric velocity of 50±2 km s^{-1}). Based on this we find that the blue- and redshifted velocity-integrated intensities of the ^{12}CO(2→1) line profile differ by ≲1% and those of the ^{13}CO(2→1) line profile by ≲2%. That is, the emission is very symmetric with respect to the systemic velocity, which is also indicated by the close agreement between the intensity-weighted centre velocities and the estimated systemic velocity, see Table 2.

3.3. Line widths

Most likely none of the line components in the CO spectra originate in a symmetrically expanding circumstellar envelope, thus all inferred expansion velocities are projected velocities. The widths of the LVF in the ^{13}CO lines correspond to an expansion velocity of ∼7 km s^{-1}. The full width at half intensity of the ^{13}CO(2→1) IVF is ∼100 km s^{-1}, and the two horns in the IVF of the ^{12}CO(2→1) profile are separated by 92 km s^{-1} (i.e., an expansion velocity of ∼50 km s^{-1} can be inferred). The HVWs probably extend to about ±145 km s^{-1} on each side of the systemic velocity, and the HVFs both expand with a (projected) velocity of 132±2 km s^{-1}.

3.4. Line intensities and optical depths

In order to analyze the emission in more detail we have calculated the integrated intensity over seven velocity intervals: the LVF, the IVF regions on both sides of the LVF, the HVWs, and the HVFs, see Table 3. A measure of the uncertainties in the integrated intensities are obtained as $30T_{\rm pp,30}$, where $T_{\rm pp,30}$ is the peak-to-peak noise in spectra with a velocity resolution reduced to 30 km s^{-1}. Note that the integrated intensities in Table 3 do not necessarily come from the individual features, since there is considerable overlap in velocity space between these features, and we have made no attempt to separate them.

The CO emission is essentially unresolved at a resolution of ∼20″. Thus, the high and nearly constant 2→1/1→0 ^{12}CO intensity ratios, ∼3–4, over the entire velocity range is most likely attributed to beam dilution, assuming that the 1→0 and 2→1 line-emitting gas coincide (a not unreasonable assumption considering the similarity of the line profiles), rather than being an effect of low optical depths, in which case differences

Table 3. Line intensities and line intensity ratios in seven velocity ranges

Velocity range	Associated feature	^{12}CO(1–0) [Kkm/s]	^{12}CO(2–1) [Kkm/s]	$\frac{2-1}{1-0}$	^{13}CO(1–0) [Kkm/s]	^{13}CO(2–1) [Kkm/s]	$\frac{2-1}{1-0}$	$\frac{^{12}\mathrm{CO}}{^{13}\mathrm{CO}}$(1–0)	$\frac{^{12}\mathrm{CO}}{^{13}\mathrm{CO}}$(2–1)
–110 → –80	bHVF	0.7	1.8	2.7	0.11:	0.6	5.3:	5.8:	2.9
–80 → –10	bHVW	2.6	7.3	2.8	0.24	1.3	5.3	10.7	5.8
–10 → 35	bIVF	2.8	9.9	3.5	1.1	3.7	3.3	2.5	2.7
35 → 45	LVF	0.6	2.2	3.6	0.40	1.4	3.6	1.5	1.5
45 → 90	rIVF	2.7	9.6	3.5	1.0	4.4	4.4	2.7	2.2
90 → 160	rHVW	2.2	7.5	3.5	0.25	1.2	4.6	8.5	6.5
160 → 190	rHVF	0.8	2.7	3.5	0.21	0.7	3.1	3.6	4.2
	$30T_{\mathrm{pp},30}$	0.16	0.15		0.10	0.12			

in the excitation conditions in the different regions should show up. The ^{13}CO lines also have a fairly constant intensity ratio, only marginally higher than the ^{12}CO ratio, ∼3–5, indicating relatively high optical depths also in these lines. There is a clear trend in the ^{12}CO/^{13}CO line intensity ratio in the sense that the emission in the LVF and IVF has a significantly lower ratio than the HVW emission; this applies especially to the LVF. The HVFs may also have a lower ratio (in particular, if one subtracts the line wing emission in this velocity range). This suggests lower optical depths in the high velocity emission.

3.5. The ^{12}CO(2 → 1) brightness distribution

We will here concentrate on the ^{12}CO(2 → 1) map data since they have a much higher quality than the ^{12}CO(1 → 0) map data. We have produced brightness distribution maps in 20 $\mathrm{km\,s^{-1}}$-intervals centred at –90, –70, ..., 170 $\mathrm{km\,s^{-1}}$, Fig. 2. In each velocity interval the emission is unresolved with a HPBW=23″. The maxima of the brightness distributions in the central part of the emission, -20 to 100 $\mathrm{km\,s^{-1}}$, lie within a radius of 1″ of each other, Fig. 3 [this is not an effect of the way we centred the maps with respect to each other; we will in the following discussions assume that the central star coincides in position with the (0,0)-position)]. However, for the higher-velocity emission maxima there is a clear trend: they are displaced with respect to the centre along a PA∼90°, with the blueshifted emission to the W and the redshifted emission to the E in a very symmetric way. The separation between the HVFs is ∼9″. Furthermore, the velocities are clearly (essentially linearly) increasing (in an absolute sense with respect to the centre velocity) with increasing offset, Fig. 4.

4. Interpretation

4.1. The structure of the molecular envelope

We are most likely witnessing a former AGB-envelope where the bulk of the gas has been accelerated to (much) higher velocities by a high-velocity post-AGB wind that is inherently bipolar or that has been channelled by a dense disk, as e.g. in the post-AGB object M1-92 (Bujarrabal et al. 1994, 1997, 1998). The HVWs and the HVFs would then correspond to the gas in the polar directions that has been accelerated to the highest velocities, as e.g. in M1-92 and another (probable) post-AGB object OH231.8+4.2 (Alcolea et al. 1996). This is certainly consistent with the brightness distributions, Figs. 2, 3 and 4, where IVF emission still comes from a region close to the star, while the high-velocity gas seem to outline a bipolar outflow with a velocity increasing linearly with distance from the centre (∼30 $\mathrm{km\,s^{-1}}$ arcsec^{-1}; the results for M1-92 and OH231.8+4.2 are ∼8 and ∼7 $\mathrm{km\,s^{-1}}$ arcsec^{-1}, respectively). The IVF probably originates from the equtorial regions of the former AGB-envelope. Below we will discuss the interpretation of the individual features and Fig. 5 shows a cartoon of a possible model for the source.

The LVF in the ^{13}CO spectra, for which we lack spatial information, can be fitted with a parabolic line shape with ∼14 $\mathrm{km\,s^{-1}}$ full width at the base, i.e., an expansion velocity of ∼7 $\mathrm{km\,s^{-1}}$ if there are no projection effects. The ^{12}CO/^{13}CO line intensity in this velocity range is so low, ∼1.5, that the optical depths must be very high. It is not clear why this feature is not clearly seen in the ^{12}CO lines. The most reasonable explanation is high optical depths in these lines (see Sect. 4.2). This suggests that the LVF originates in very dense gas, probably close to the star. Very similar features are present in the CO spectra of M1-92 (Bujarrabal et al. 1994, 1997), and the (probable) post-AGB object HR3126 (Nyman et al. 1998), where also the ^{12}CO/^{13}CO line intensity ratios are low, ∼2. Similar, but much narrower, features are seen towards the post-AGB objects 89 Her (Alcolea & Bujarrabal 1991; also here the ^{12}CO/^{13}CO line intensity ratio is low, ∼2) and the Red Rectangle (Jura et al. 1995). Except for 89 Her, a disk structure is regarded as the most likely explanation in these cases, and in M1-92 the emission is actually resolved (Bujarrabal et al. 1998). In fact, also towards normal AGB-stars such (very narrow) features in the CO spectra are not uncommon (Knapp et al. 1998), and they are interpreted as being due to varying wind characteristics with time, perhaps connected to thermal pulses (Knapp et al. 1998), or a disk channelling a bipolar outflow in the one case where data with sufficient spatial resolution exist (Kahane & Jura 1996). We cannot at this point exclude that the LVF originate from an AGB-envelope gas that has not experienced additional acceleration.

The IVF may originate in the outer parts of the disk, whose inner, denser parts are traced by the LVF, or in a separate component. Since this part of the CO emission is unresolved in our

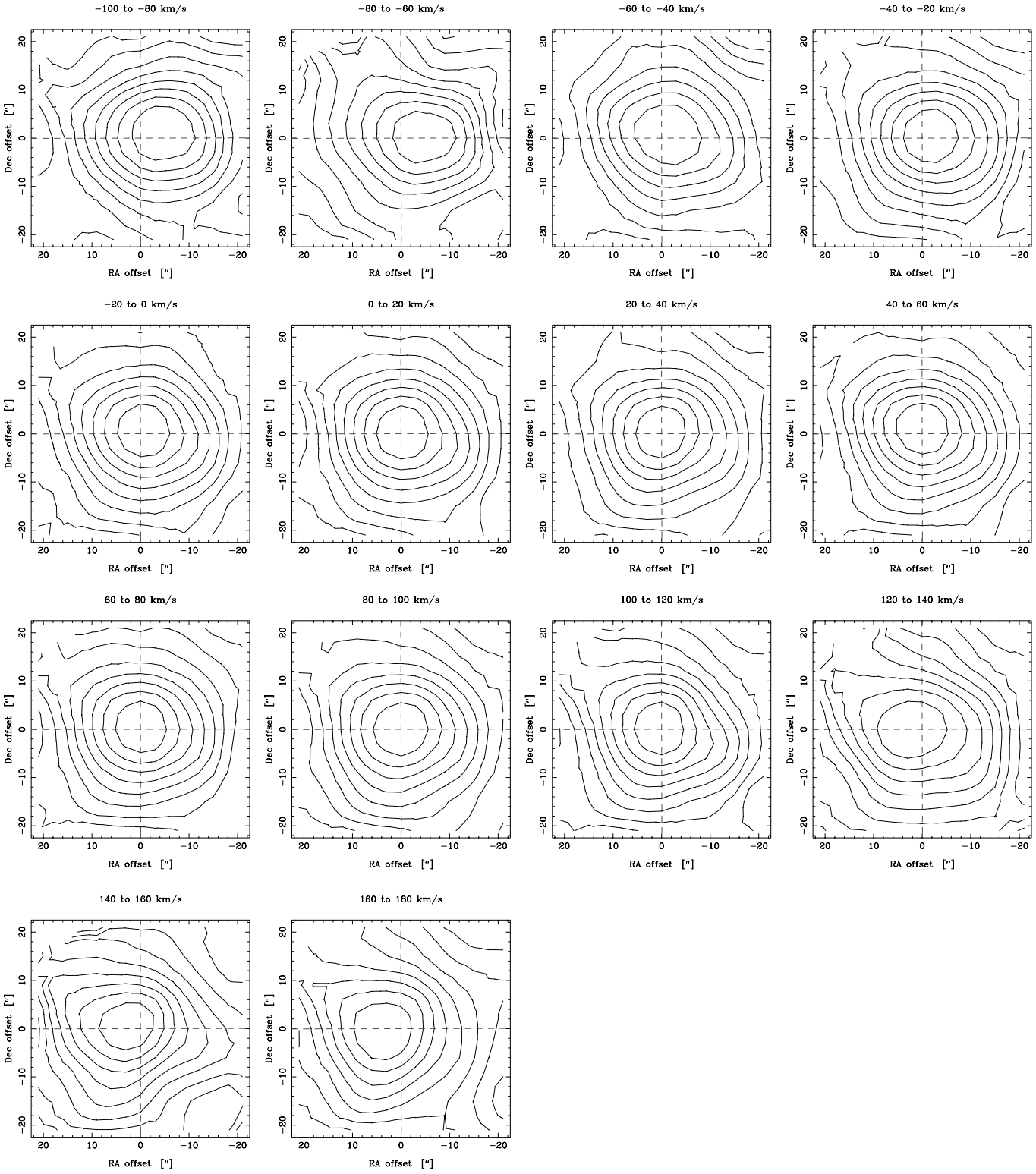

Fig. 2. ^{12}CO(J=2→1) brightness distributions in 20 km s^{-1}-intervals centred at –90, –70, ..., 170 km s^{-1}. The contours represent 10%, 20%, ..., 90% of the maximum intensity in each panel

observations we do not have any spatial information, but we can use the high-resolution OH maser observations by te Lintel Hekkert et al. (1992) to discuss the structure of this component. We believe that the OH masers and the IVF of the CO emission originate in the same region because their velocity ranges agree very well, and there is no OH emission at velocities corresponding to LVF, possibly indicating that the densities in this region are high enough to collisionally quench the

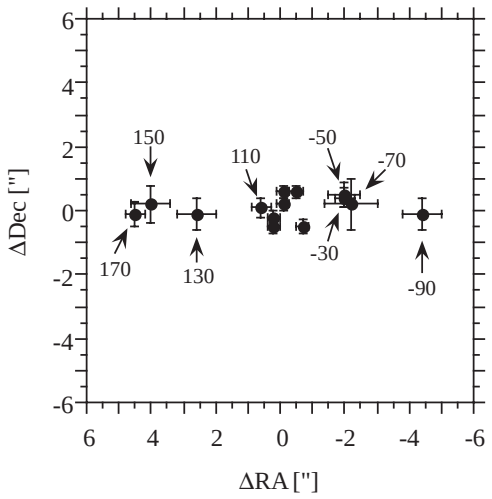

Fig. 3. Positions of the ^{12}CO(J=2$\rightarrow$1) brightness maxima, in 20 km s^{-1}-intervals centred at –90, –70, ..., 170 km s^{-1}, with respect to the position of the total brightness maximum

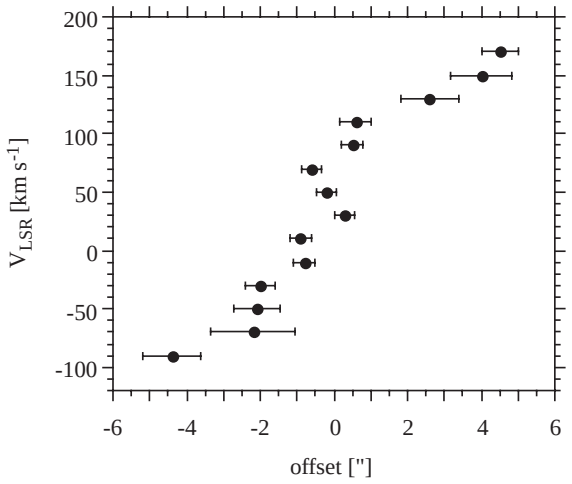

Fig. 4. Offsets of the ^{12}CO(J=2$\rightarrow$1) brightness maxima, in 20 km s^{-1}-intervals centred at –90, –70, ..., 170 km s^{-1}, with respect to the position of the total brightness maximum [positive (negative) offset for a point lying on the east (west) side of a line with PA=0°]

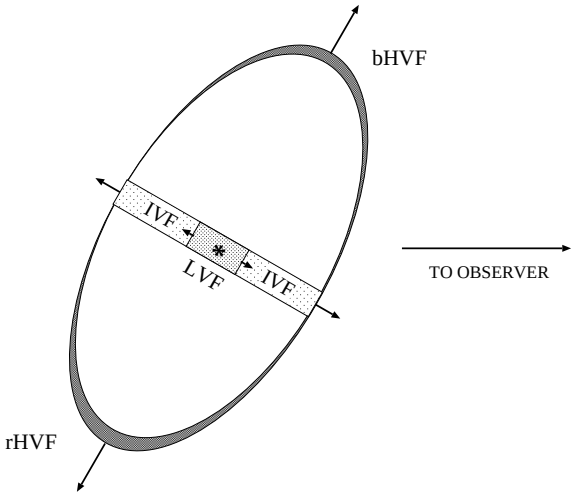

Fig. 5. Cartoon of a possible model for the molecular envelope of HD101584

OH maser. The OH emission traces an apparent bipolar structure whose expansion velocity increases almost linearly with the distance from the centre. However, we do not believe that the OH masers are associated with the high-velocity CO outflow because their bipolar structure is not precisely aligned with the high-velocity CO emission, it has a smaller velocity gradient ($\sim$20 km s^{-1} arcsec^{-1} compared to $\sim$30 km s^{-1} arcsec^{-1}), and, in particular, it expands in the opposite direction. The most attractive explanation to this is that the OH emission originates in the plane (or at low latitudes) of an expanding disk perpendicular to the CO outflow [an interpretation supported by the OH observations of M1-92 (Seaquist et al. 1991) and the planetary nebula Roberts 22 (Sahai et al. 1999)]. In this way the opposite expansion direction may be explained by a purely geometrical effect (see Fig. 5). If the OH masers are located in a disk it is required that the disk has a velocity gradient (there may also be a latitudinal velocity dependence), and that it is seen more edge-on than face-on (with the major axis approximately in the N-S direction). The latter provides a welldefined axi-symmetry, and may explain the alignment of the OH maser spots in terms of larger amplification paths in the radial direction than in the tangential direction, while the former results in the (linear) increase in the velocity of the OH masers with angular distance from the star. An upper limit to the inclination angle of the disk (with respect to the line-of-sight) can be obtained by noting that the true size of the OH emission (the apparent size is $\sim$4″) is very likely smaller than the size of the central CO emission ($\lesssim$15″ as estimated from our map data). This results in an inclination angle $\lesssim$75°, but this estimate must be regarded as very uncertain. If the disk and the outflow are perpendicular, the maximum velocity in the outflow lies in the range 150–550 km s^{-1}. Another, but less likely, explanation to the apparent different outflow directions of the OH and CO emissions is that the outflow is directed almost along the line of sight, and that some precessional motion is present.

The relation between the putative disk, responsible for the LVF, and the putative disk, responsible for the OH emission and the IVF, is unclear. If the major fraction of the IVF emission emanates from the former AGB envelope one would expect this region to have the structure of a (thick) toroid. Since the outflow velocities in the IVF are much higher than that normally found in AGB-envelopes, a large fraction of the gas in the former AGB-envelope must have been substantially accelerated.

The IVF of the ^{12}CO(2$\rightarrow$1) emission also shows two horns, giving the line profile a double-peaked appearance. The horns are not visible in the ^{13}CO(2$\rightarrow$1) profile. In velocity they are located almost exactly at the edges of the main component of the ^{13}CO(2$\rightarrow$1) emission. We note here that the HD101584 ^{12}CO line profiles to a large extent qualitatively resemble those of the carbon star V Hya, except for the LVF and the HVFs (Kahane et al. 1996; Knapp et al. 1997). It is interesting though that Kahane et al. and Knapp et al. differ in their interpretations.

The Knapp et al. scenario is the one most similar to ours, and they interpret the horns as arising preferentially from regions close to the minor axis of a flattened structure (with roughly the same expansion velocity in all directions) inclined towards the line of sight. In our case the horns lie close to the edge of the IVF suggesting that the flattened structure is seen almost edge-on. The geometry/kinematics combined with optical depth effects could possibly explain why the horns are not seen in the ^{13}CO emission.

The HVWs most likely correspond to gas participating in a bipolar high-velocity outflow since the red- and blueshifted wings are clearly spatially separated (Figs. 3 and 4). The linear relation between velocity and displacement from the centre is most easily explained as due to a relatively short period of acceleration after which the gas has been expanding freely (i.e., the highest velocities reaches the largest distances in a given time), but it can also be due to the interaction between a fast bipolar wind running into a slow wind (e.g., Icke 1988). The HVFs at the edges of the line wings suggest that a fair fraction of the high-velocity gas somehow has reached a well defined terminal velocity, which to within a few% is the same on the opposite sides of the star. Such marked features have not been seen in any other post-AGB object with high-velocity winds, although similar, but much weaker, features may be present in the ^{12}CO($2\rightarrow1$) data obtained towards OH231.8+4.2 (Alcolea et al. 1996). It is not obvious how gas being so strongly accelerated (probably by an order of magnitude) in two opposite directions will reach close to exactly the same terminal velocity. It is tempting to assign these features to emission from gas in interaction zones, between a fast outflow and a slowly moving AGB-wind, in the polar regions. The very similar expansion velocities of the HVFs could, as an alternative, suggest that this matter has been ejected at high velocities by some mechanism [we note here that in their spectral appearance these features resemble the "bullet"-features observed in bipolar outflows of young stars, that may be effects of episodic mass ejection (Bachiller & Cernicharo 1990)]. Despite not knowing whether one or several mass loss events created the high-velocity outflow we may crudely estimate size and time scales by adopting a very uncertain distance of 1 kpc (assuming a post-AGB object, Bakker et al. 1996b). The HVFs lie at a projected distance of $\sim7\times10^{16}$ cm from the centre. The dynamical time scale is $170\times\cot\theta$ yr (where θ is the angle between the line-of-sight and the outflow axis, i.e., the same as the inclination angle of the putative disk introduced above; we assume here that the velocity does not change with radius and that the gas starts close to the star), i.e., the high-velocity outflow could be as young as $\sim$50 yr (the disk is seen almost edge-on), but also an age approaching 10^3 yr (the disk is seen almost face-on) is possible.

A high-velocity outflow is traced also in the broad P Cygni-profiles of the Balmer lines (Bakker et al. 1996b). These indicate expansion velocities of $\sim100\,\mathrm{km\,s^{-1}}$, suggesting that the CO high-velocity outflow is an effect of the present mass loss. Low-excitation optical emission and absorption lines are interpreted as arising in a circumsystem disk that is viewed almost edge-on, i.e., the same orientation that we infer for the region responsible for the CO IVF and the OH emission. It is tempting to assign the LVF to the inner regions of this disk.

4.2. The ^{12}CO/^{13}CO-ratio

There are significant, and systematic, variations in the ^{12}CO/^{13}CO line intensity ratios within the line profiles. The IVF, and in particular the LVF, and probably the HVFs have low ratios, $\sim$1.5–3, while the ratios in the HVWs are higher by at least a factor of $\sim$2–3. A change in the stellar ^{12}C/^{13}C-ratio as a function of time may in principle play a rôle, but this seems less likely in this case. We believe that the variation mainly reflects changes in optical depth. This makes the estimate of the ^{12}CO/^{13}CO-ratio very uncertain, but we expect it to be $\gtrsim$10 (the maximum line intensity ratio found in the line wings, see Table 3).

Assuming that a ^{12}CO/^{13}CO abundance ratio of 10 applies also to the gas in the LVF and the IVF, and that there is no difference in the excitation of the two isotopic variants, we estimate optical depths for these components of $\sim$0.5 and $\sim$5 in the ^{13}CO($2\rightarrow1$) and ^{12}CO($2\rightarrow1$) lines, respectively, from a line intensity ratio of $\sim$2.

We note here that HD101584 shares the characteristic of a low ^{12}CO/^{13}CO line intensity ratio with a number of other (candidate) post-AGB objects: the O-rich objects 89 Her (Alcolea & Bujarrabal 1991), OH231.8+4.2 (Alcolea et al. 1996), M1-92 (Bujarrabal et al. 1997), and HR3126 (Nyman et al. 1998), and the C-rich objects M1-16 (Sahai et al. 1994), and the Boomerang nebula (Sahai & Nyman 1997). In M1-92 and OH231.8+4.2 the ^{12}CO/^{13}CO line intensity ratio also markedly decrease towards the line centre, and in the case of M1-92 the interferometric mapping shows that the low intensity ratio arises from material at the centre of the nebula (as seems to be the case also in HD101584, see Sect. 3.5), and that it is most likely due to a higher optical depth in this gas.

4.3. The mass of the molecular envelope

We can make a crude estimate of a lower limit to the mass of the molecular material, assuming LTE-excitation and optically thin and unresolved emission, using the formula,

$$M = \frac{16\pi k m_{\rm H}}{hcg_{\rm u}A_{\rm ul}f_{\rm CO}}\,\frac{D^2}{A_{\rm e}}\,I\,Q(T_{\rm ex})\,e^{E_{\rm u}/kT_{\rm ex}} \qquad (1)$$

where the normal symbols have been used for the constants, and $f_{\rm CO}$ is the abundance of CO with respect to H_2, D is the distance, $A_{\rm e}$ is the effective telescope area, I=$\int T_{\rm mb}dv$, Q is the partition function, $T_{\rm ex}$ is the excitation temperature, and $E_{\rm u}$ is the energy of the upper level. Using the ^{13}CO($2\rightarrow1$) line, $f_{^{13}{\rm CO}}$=0.1$f_{\rm CO}$ (where $f_{\rm CO}$=3×10^{-4}, a value appropriate for an O-rich envelope), and $T_{\rm ex}$=15 K (see the analysis of the CO emission from M1-92, Bujarrabal et al. 1997; furthermore if the ($2\rightarrow1$)/($1\rightarrow0$) intensity-ratio of the ^{13}CO-lines is mainly attributed to beam filling the temperature must be low since the ^{13}CO optical depths appears to be less than one), we obtain $M>0.1\,{\rm M}_\odot$. This is much less than the envelope mass estimated

from the IR emission ($2\,M_\odot$), suggesting that either the dust mass estimate is severely in error, or the dust and CO emission come from different regions. We regard it as unlikely that the CO mass is severely underestimated, unless a fair fraction of the CO molecules are photodissociated (if so, predominantly by the interstellar UV radiation).

We can also make a crude estimate of a lower limit to the final AGB mass loss rate. At least half of the emission (corresponding to $>0.05\,M_\odot$) comes from a region smaller than $\sim5''$ in radius (corresponding to a time scale of 1000 years if we assume an AGB wind velocity of $20\,\mathrm{km\,s^{-1}}$). Thus, the AGB mass loss rate must have been well above $10^{-5}\,M_\odot\,\mathrm{yr}^{-1}$ during the final evolution, and maybe considerably more if a major fraction of the original CO is photodissociated.

4.4. The wind momentum

A crude lower limit (e.g., no correction for inclination) to the (excess) momentum of the gas that has been accelerated to velocities above that of the AGB wind is obtained by applying Eq. (1) to the gas outside the central $\pm20\,\mathrm{km\,s^{-1}}$ (of the systemic velocity) in $10\,\mathrm{km\,s^{-1}}$-intervals and by multipying with the velocity increase (i.e., the average velocity in the $10\,\mathrm{km\,s^{-1}}$-interval minus $20\,\mathrm{km\,s^{-1}}$). The result is $\sim5\times10^{38}\,\mathrm{g\,cm\,s^{-1}}$. This corresponds to the total momentum supplied by a radiation luminosity of $\sim10^4\,L_\odot$ in 10^4 yr [i.e., an order of magnitude longer than the (rough) estimate of the maximum dynamical age of the high-velocity gas]. Even though the estimate is crude, it clearly points towards a mechanism different than that of a radiation-driven wind. Bujarrabal et al. (1998) found a similar situation for M1-92, and they suggest an accretion-driven wind.

4.5. The SiO and HCN data

Neither SiO nor HCN emission was detected despite a relatively sensitive search. The line intensity ratios are: SiO($3\rightarrow2$)/CO($1\rightarrow0$) $<$ 0.07 and HCN($1\rightarrow0$)/CO($1\rightarrow0$) $<$ 0.06. The SiO/CO-ratio is very low for a normal O-rich AGB-envelope, and the HCN/CO-ratio is very low for a normal C-rich AGB-envelope [Olofsson et al. 1998; note that we expect the SiO($3\rightarrow2$)/CO($1\rightarrow0$)-ratio to be higher than the SiO($2\rightarrow1$)/CO($1\rightarrow0$)-ratio]. Considering the detection of an OH maser and a possible detection of a 10 μm dust feature, the most reasonable explanation to our results is that the envelope is O-rich but that presently there is very little gas left in the inner regions of the envelope where SiO is normally excited. We note here also the marked difference with OH231.8+4.2 towards which a large number of molecular species have been detected (Morris et al. 1987; Lindqvist et al. 1992; Sánchez-Contreras et al. 1997).

5. Conclusions

The most reasonable explanation to our results is that HD101584 has recently left the AGB during which it experienced a final intense ($>10^{-5}\,M_\odot\,\mathrm{yr}^{-1}$), and highly (possibly axi-) symmetric mass loss (as inferred from the very symmetric line profiles). There remains $>0.1\,M_\odot$ of molecular gas around the star from this period. A very efficient acceleration to $\sim50\,\mathrm{km\,s^{-1}}$ of a substantial fraction of this gas has occurred. About 25% of the gas has been accelerated to very high velocities ($>50\,\mathrm{km\,s^{-1}}$) in a bipolar outflow with maximum velocities in excess of $130\,\mathrm{km\,s^{-1}}$ (and possibly as high as $\sim500\,\mathrm{km\,s^{-1}}$ depending on the uncertain inclination angle), causing the original AGB-envelope to be stretched out in the polar regions. The linear increase in outflow velocity with distance from the source centre suggests either a short period of intense acceleration a few hundred years ago (as estimated from the dynamical age), or a fast wind blowing through the slower AGB-envelope. In this scenario the bulk of the CO emission and the OH emission originate from the higher-density equatorial region (taking the form of a disk or a toroid). The data suggest that a substantial velocity gradient has been set up also in this gas, and the OH emission originates from regions closer to the star than does the CO emission. The plane of the disk/toroid lies almost exactly in the N-S direction, and the bipolar outflow points away from us to the E and towards us to the W. The inclination of the disk/toroid with respect to the line-of-sight is not easily estimated. There are arguments for both a small inclination angle (the high expansion velocities, the star is clearly visible in the UV/optical region), and a large inclination angle (the structure of the OH and CO emission, the optical absorption lines). We favour the latter and estimate a crude upper limit to the inclination angle of $\sim75^\circ$. Therefore, the dynamical age of the outflow may be as low as ~50 yr, in which case time variations in both the stellar and circumstellar spectra should be observable. However, much higher spatial resolution observations are required to resolve the true configuration, and we refrain from more speculation on this issue. It is also possible that the dynamical age only provides a lower limit to the outflow time scale, since the escaping material may, for some reason, be observable in CO emission only within a certain distance of the star. The momentum of the high-velocity gas is so high that it precludes a radiation-driven wind. A narrow, central feature, prominent in the ^{13}CO lines, suggests the existence of high-density gas, presumably close to the star. This could be the circumbinary disk inferred from optical and infrared data.

Acknowledgements. Financial support from the Swedish Natural Science Research Council (NFR) is acknowledged. We are grateful to the referee, Dr. J. Alcolea, for valuable comments on the manuscript.

References

Alcolea J., Bujarrabal V., 1991, A&A 245, 499
Alcolea J., Bujarrabal V., Sánchez Contreras C., 1996, A&A 312, 560
Bachiller R., Cernicharo J., 1990, A&A 239, 276
Bakker E.J., Lamers H.J.G.L.M., Waters L.B.F.M., Waelkens C., 1996a, A&A 310, 861
Bakker E.J., Lamers H.J.G.L.M., Waters L.B.F.M., et al., 1996b, A&A 307, 869
Bujarrabal V., Alcolea J., Neri R., Grewing M., 1994, ApJ 436, L169
Bujarrabal V., Alcolea J., Neri R., Grewing M., 1997, A&A 320, 540

Bujarrabal V., Alcolea J., Neri R., 1998, ApJ 504, 915
Humphreys R.M., 1976, ApJ 206, 122
Icke V., 1988, A&A 202, 177
Jura M., Balm S.P., Kahane C., 1995, ApJ 453, 721
Kahane C., Audinos P., Barnbaum C., Morris M., 1996, A&A 314, 871
Kahane C., Jura M., 1996, A&A 310, 952
Knapp G.R., Jorissen A., Young K., 1997, A&A 326, 318
Knapp G.R., Young K., Lee E., Jorissen A., 1998, ApJS 117, 209
Lindqvist M., Olofsson H., Winnberg A., Nyman L.-Å., 1992 A&A 263, 183
Loup C., Forveille T., Nyman L.-Å., Omont A., 1990, A&A 227, L29
Morris M., Guilloteau S., Lucas R., Omont A., 1987, ApJ 321, 888
Nyman L.-Å., Olofsson H., Rogers C., Heske A., Sahai R., 1998, in prep.
Olofsson H., Lindqvist M., Nyman L.-Å., Winnberg A., 1998, A&A 329, 1059
Oudmaijer R.D., Waters L.B.F.M., van der Veen W.E.C.J., Geballe T.R., 1995, A&A 299, 69
Parthasarathy M., Pottasch S.R., 1986, A&A 154, L16
Sahai R., Nyman L.-Å., 1997, ApJ 487, L155
Sahai R., Wootten A., Schwarz H.E., Wild W., 1994, ApJ 428, 237
Sahai R., Zijlstra A.A., Bujarrabal V., te Lintel Hekkert P., 1999, AJ, in press
Sánchez Contreras C., Bujarrabal V., Alcolea J., 1997, A&A 327, 689
Seaquist E.R., Plume R., Davis L.E., 1991, ApJ 367, 200
te Lintel Hekkert P., Chapman J.M., Zijlstra A.A., 1992, ApJ 390, L23
Trams N.R., van der Veen W.E.C.J., Waelkens C., Waters L.B.F.M., Lamers H.J.G.L.M., 1990, A&A 233, 153
van der Veen W.E.C.J., Trams N.R., Waters L.B.F.M., 1993, A&A 269, 231
Waters L.B.F.M., Waelkens C., Trams N.R., 1993, High Latitude Supergiants. In: Schwarz H.E. (ed.) Mass Loss on The AGB and Beyond. ESO Conference and Workshop Proceedings No. 46, Chile, p. 298